Green Chemistry

PAPER

View Article Online
View Journal | View Issue



Cite this: *Green Chem.*, 2026, **28**, 9013

# Electrochemical ammonia oxidation using nickel copper hydroxide with $H_2$ recovery at high current density and selectivity

D. D. van Noordenne, P. J. Jungbacker, A. Urakawa and F. M. Mulder *

Received 18th December 2025,
Accepted 27th April 2026

DOI: 10.1039/d5gc06877k

rsc.li/greenchem

Electrochemical conversion of ammonia has received increasing attention due to the potential applications for fertiliser production and wastewater treatment. This work demonstrates the application of a homogeneously copper-doped nickel hydroxide, prepared through an easily scalable precipitation method, as an electrochemical oxidation catalyst. A cation exchange membrane divides the cell and prevents re-reduction of the oxidation product. During chronopotentiometry $Ni_{0.8}Cu_{0.2}(OH)_2$ was able to perform ammonia oxidation, with limited oxygen evolution, from 2.5 mA $cm^{-2}$ up to 400 mA $cm^{-2}$. The faradaic efficiency for nitrite formation increased with the applied current density. At a high initial ammonia concentration of 1 M, $Ni_{0.8}Cu_{0.2}(OH)_2$ converted 77% of the ammonia in less than 3.5 hours, applying a high current density of 400 mA $cm^{-2}$. This resulted in a faradaic efficiency of 96% total, which is 91% $NO_2^-$ and 5% $NO_3^-$, which would be impossible in an undivided cell. Therefore, this work demonstrates the potential for efficient and selective ammonia oxidation towards nitrite under industrially relevant current density and conditions.



**Green foundation**

1. The electrochemical oxidation of ammonia at high selectivity to nitrite and at industrially relevant current densities is presented, with coproduction of green hydrogen for recovery of energy.
2. Nitrogen oxides and salts are used intensively as fertilisers and chemical feedstocks and provide about four times higher value per nitrogen unit than ammonia. When produced using green electrons, these materials can be obtained in a green manner.
3. It is shown that high ammonia concentrations in 1 M KOH electrolyte can be utilised, going beyond concentrations encountered in wastewater treatment. A cation exchange membrane cell design with $Ni_{0.8}Cu_{0.2}OOH$ as the active catalyst effectively protects the oxidation products from undesirable reduction.

## Introduction

Humanity relies on the production of synthetic fertilizers to sustain the growing population.[1] In 2021, 187 million tons of ammonia was produced, with 147 million tons used for synthetic fertilizer manufacture. While ammonia is mainly used directly in fertilizer production, a significant amount is converted to nitric acid. This conversion resulted in 70 million tons of nitric acid in 2021.[2] Most of the nitric acid is combined with ammonia to produce synthetic ammonium nitrate fertilizers.

As renewable energy is increasingly implemented, increasing interest exists in producing ammonia and nitric acid electrochemically. Nonetheless, direct electrochemical ammonia production from nitrogen gas and water has yet to reach significant and reproducible synthesis rates, compared to the optimized Haber–Bosch process.[3–6] The main challenge is the difficulty of dinitrogen activation, before even being able to optimize the process. However, it would be more feasible to replace the subsequent ammonia oxidation to nitrite or nitrate using electrochemistry as one then starts from more electrochemically active ammonia. Currently, large-scale conversion is performed in the multistep Ostwald process, starting with oxidation with $O_2$ at 10 bar and 800 °C with a Pt/Rh gauze.[7,8] The formed NO is cooled down and reacted with the remaining oxygen to form $NO_2$. This $NO_2$ is absorbed with water to form nitric acid. As an alternative in this last step, the application of a hydroxide solution results in nitrite salt rather than the commonly produced nitric acid.[9] In comparison with these process conditions, electrochemistry could make it feasible to produce nitrite and nitrate with more benign conditions and a catalyst consisting of more Earth-abundant

*Chemical Engineering, Faculty of Applied Sciences, Delft University of Technology, 2629 HZ Delft, The Netherlands. E-mail: f.m.mulder@tudelft.nl*

elements. Furthermore, local application of the product, combined with small-scale ammonia, aligns with distributed renewable electricity generation. Local production and application could reduce the transport costs of both electricity and chemical products. Therefore, it is interesting to investigate electrochemical ammonia oxidation.

The electrochemical ammonia oxidation reaction (AOR) has been reported for various applications, such as fuel cells and wastewater treatment.[10–18] In these fields, noble metals are commonly used to achieve high selectivity and conversion to $N_2$ (eqn (1)). Recent research has shifted focus toward converting ammonia to nitrite (eqn (2)) and nitrate (eqn (3)).[19–22] The oxidation potentials are presented in SI Note S1. The applied conditions, such as concentration, faradaic efficiency (FE) and current density, vary significantly in the literature due to the aim to recover ammonia and nitrate from various wastewater streams (Table S1). Nickel is of significant interest as a precious metal-free catalyst that can achieve high efficiency and selectivity. Furthermore, nickel is corrosion resistant due to the stability of its solid oxidised species under alkaline and oxidative conditions. The active form is NiOOH, which can either react electrocatalytically (eqn (4)) or result in indirect oxidation with the reformation of $Ni(OH)_2$ (eqn (5)) and subsequent reoxidation of $Ni(OH)_2$ to NiOOH (eqn (6)).[23] The competing OER reaction and potential above which it can take place is also given (eqn (7)). At the counter electrode, water reduction produces $H_2$ and $OH^-$ (eqn (8)).

$$\mathrm{NH_{3(aq)} + 3\ OH^- \rightleftharpoons \frac{1}{2}N_2 + 3H_2O + 3e^-} \quad E^\circ = -0.77\,\mathrm{V}\ vs.\ \mathrm{SHE},\quad \mathrm{pH\,14} \tag{1}$$

$$\mathrm{NH_{3(aq)} + 7OH^- \rightleftharpoons NO_2^- + 5H_2O + 6e^-} \quad E^\circ = -0.17\,\mathrm{V}\ vs.\ \mathrm{SHE},\quad \mathrm{pH\,14} \tag{2}$$

$$\mathrm{NH_{3(aq)} + 9OH^- \rightleftharpoons NO_3^- + 6H_2O + 8e^-} \quad E^\circ = -0.13\,\mathrm{V}\ vs.\ \mathrm{SHE},\quad \mathrm{pH\,14} \tag{3}$$

$$\mathrm{NiOOH + NH_3 \rightarrow NiOOH + X + nH^+ + ne^-} \tag{4}$$

$$\mathrm{6NiOOH + NH_3 + H_2O + OH^- \rightarrow 6Ni(OH)_2 + NO_2^-} \tag{5}$$

$$\mathrm{Ni(OH)_2 + OH^- \rightleftharpoons NiOOH + H_2O + e^-} \quad E^\circ = 0.49\,\mathrm{V}\ vs.\ \mathrm{SHE},\quad \mathrm{pH\,14} \tag{6}$$

$$\mathrm{4OH^- \rightleftharpoons O_2 + 2H_2O + 4e^-} \quad E^\circ = +0.40\,\mathrm{V}\ vs.\ \mathrm{SHE},\quad \mathrm{pH\,14} \tag{7}$$

$$\mathrm{2H_2O + 2e^- \rightleftharpoons H_2 + 2OH^-} \quad E^\circ = -0.83\,\mathrm{V}\ vs.\ \mathrm{SHE},\quad \mathrm{pH\,14} \tag{8}$$

The layered nickel hydroxide structures have been doped with various metals to improve their properties.[19,21,24–26] The most promising approach is the addition of copper to the nickel hydroxide, resulting in a catalyst that is highly active for ammonia oxidation. For example, Jiang *et al.* reported selectivity up to 99% towards nitrite for wastewater denitrification under relevant conditions of 1 mM $NH_3$ and 0.1 M KOH electrolyte.[20] However, they presented and analysed a nanostructured phase separated catalyst material of $Ni(OH)_2$ and $Cu(OH)_2$. Possibly at the interface of these materials, there could be an activity enhancing phase compared to the two pure phases.

In our research, we found that it is possible to produce a homogeneous Cu doped $Ni_{1-x}Cu_x(OH)_2$ phase. Compared to the heterogenous mixture, one may expect that now all the material has the influence of Cu doping and this could thus result in improved activity with respect to the pure and inhomogeneously Cu-doped $Ni(OH)_2$ catalysts. Here, we report the application of a homogenously copper-doped nickel hydroxide electrode, $Ni_{0.8}Cu_{0.2}(OH)_2$.

Besides the catalyst, the experimental cell can significantly influence the results achieved with the AOR, which is commonly performed in a single cell compartment. In such a configuration, the formed nitrite and nitrate anions remain dissolved in the electrolyte and are reducible at the counter electrode to $NH_3$ and $N_2$ (Fig. 1a). To prevent this, it will be shown that a cation exchange membrane (CEM) should be applied to prevent such anion crossover and re-reduction of the oxidation products (Fig. 1b). Within this study, we shall establish the advantages of applying a divided CEM cell for the AOR compared to an undivided cell and also show the high conversion and current densities that can be achieved with the homogeneous $Ni_{0.8}Cu_{0.2}(OH)_2$ catalyst. The CEM appears crucial to achieve high product selectivity and FE and to determine the FE unambiguously. Furthermore, we show that it becomes possible to work with concentrated ammonia solutions and current densities up to 400 mA $cm^{-2}$.

## Experimental

All chemicals were obtained from Sigma-Aldrich and were used as purchased. All water mentioned is Mili-Q water with a conductivity of <0.1 μS $cm^{-1}$. A 28 wt% $NH_3$ concentrated solution was used. A high concentration solution of ammonia in 1 M KOH was prepared by slowly mixing the appropriate KOH solution and 28 wt% $NH_3$. The resulting solution was kept in a closed container to minimize ammonia losses.

### Synthetic procedures

To obtain a homogeneously mixed Ni–Cu phase material, a previously reported co-precipitation method was used and modified for the addition of Cu instead of Fe.[27] An aqueous solution containing $NiSO_4{\cdot}6H_2O$ (0.25 M, 50 mL, 20.6% Ni) with the corresponding amount of $CuSO_4$ (0.0625 M, 99%) was prepared to obtain the $Ni_{0.8}Cu_{0.2}(OH)_2$ material. Under vigorous stirring of the KOH (2.0 M, 100 mL) solution, the metal precursor solution was added dropwise. The precipitate was collected by centrifugation (3500 rpm, 10 min) and after washing twice with water and once with ethanol. The residue was dried at 50 °C under vacuum. Ball milling at 200 rpm for 15 min resulted in a powdered material for preparing the electrodes.

 

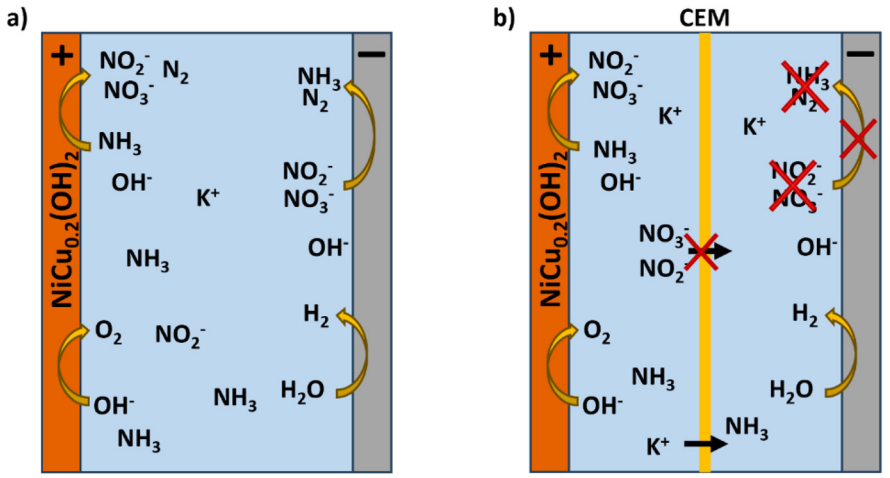


**Fig. 1** The difference between performing the AOR in an alkaline electrolyte within (a) an undivided cell and (b) a cell divided with a cation exchange membrane. The ionic current can be carried by $K^+$, while the product anions $NO_2^-$ are blocked. $NH_3$ in the feed can only react at the positive electrode. At alkaline pH, $NH_3$(aq) remains.

### Material characterisation

X-ray diffraction was performed using a Bruker D8 Advance ECO diffractometer equipped with a Cu-$K_\alpha$ source ($K_{\alpha1}$ = 1.54060 Å, 40 kV and 25 mA) and a Lynxeye-XE-T position sensitive detector. A fixed divergence slit was used with a Bragg–Brentano geometry. A step size of 0.02° with a measuring time of 0.1 s per step was employed. SEM and EDS were performed on both the powders and electrodes using a SEM-JEOL-6010LA.

### Electrode preparation

Electrodes were prepared by homogenously mixing the material ($Ni_{1-x}Cu_x(OH)_2$) with 50 wt% carbon super P® and 50 wt% graphite through pestling. The binder polyethersulfone (7 wt% in *N*-methylpyrrolidone) was added to obtain a slurry. The nickel foam matrices (0.5 mm thick, 99.9% Ni) were prepared by cutting 20 × 20 mm squares. These squares were cleaned in HCl (4 wt%) and acetone for 5 min each in a sonication bath. After pasting, the slurry was solidified through phase inversion in water.[28,29] Such an electrode processing method is known to result in highly porous electrodes with a large electrochemical surface area, which is advantageous for relatively high current densities. The electrodes were dried under vacuum at 50 °C.

### Electrochemical experiments

Cyclic voltammetry was performed with a Parstat MC-1000 system with a three-electrode setup. The Tafel slope and chronopotentiometric measurements were carried out using a Maccor 4000 battery cycling system. These were mainly performed in a three-electrode setup. Auxiliary potential channels could be connected to measure cell potential and the potential of the counter electrode in comparison with a second Hg/HgO reference electrode.

Cyclic voltammetry and measurements without membranes were performed in a single compartment cell with a nickel foam counter electrode and an Hg/HgO (KOH) reference electrode. Experiments with a membrane were performed with a 20 mm diameter Nafion 117 membrane in between two 50 mL electrolyte compartments. If ammonia was added, it was added on both sides of the membrane to reduce the effect of initial differences in the ammonia concentration and pH on the measurements, and to demonstrate the limited poisoning effect of ammonia on the counter electrode. Before performing ammonia oxidation during chronopotentiometry, the cell was operated at the same current density without ammonia until a stable potential was achieved. This was to stabilize the electrode in the nickel oxyhydroxide state and convert all potential nitrogen contamination[30] to nitrogen gas, nitrite, and nitrate to improve accuracy.

Cyclic voltammetry was performed in 1 M KOH in the range of 0–0.63 V *vs.* Hg/HgO at a scan rate of 1 mV $s^{-1}$. This was followed by the addition of 50 mM $NH_4OH$ and repeated. The fifth cycle was used for analysis. The Tafel slope measurements were performed by initially applying a current to convert all hydroxide in the catalytic material into oxyhydroxide before applying a constant current for 10 min at increasing current densities. A range from 0.25 mA $cm^{-2}$ up to 25 mA $cm^{-2}$ was applied, where the area refers to the geometric surface area.

### Ion chromatography

The concentration of anions in the electrode were determined using an ion chromatograph (IC). The system consisted of a Thermo Scientific™ Dionex™ Integrion™ HPIC™ system equipped with a conductivity detector and an AS18-Fast anion column. In accordance with Thermo Scientific application note 72481, AutoNeutralization™ was applied to improve accuracy by removing the KOH background without dilution. A gradient in the KOH concentration of the eluent was applied to

obtain completely separate nitrite and nitrate peaks for maximum accuracy.

## Results and discussion

X-ray diffraction (XRD) was used to confirm the formation of $Ni_{0.8}Cu_{0.2}(OH)_2$, denoted as $NiCu_{0.2}$, synthesized through a precipitation method under alkaline conditions. The same synthesis method was applied with the individual nickel and copper salt, which clearly formed two distinguishable materials (Fig. 2). The nickel precipitated as the β-$Ni(OH)_2$ phase, consistent with the reference pattern. The copper salt formed CuO, as $Cu(OH)_2$ can lose water during drying. The XRD pattern of $NiCu_{0.2}$ indicates the formation of β-$Ni(OH)_2$ with a potentially minimal peak shift, indicating the successful doping of the copper. The absence of a separated phase suggests that the Cu is homogenously incorporated.

Homogeneous incorporation of the copper was further confirmed with SEM and EDS (Fig. 3). The $NiCu_{0.2}$ particles consist of crystallites but the presence of a background indicates also an amorphous material in between. EDS analysis shows a homogeneous distribution of Ni and Cu, suggesting that copper is homogenously incorporated into the $Ni(OH)_2$. Furthermore, a Ni : Cu ratio of 0.83 : 0.17 throughout the powder was determined. This is close to the theoretical ratio. Potassium and sulphate are present as a crystalline $K_2SO_4$ contaminant from the precipitation method. This salt was further washed out during the electrode preparation (Fig. S1). Overall, these results demonstrate copper homogenously incorporated to form $NiCu_{0.2}$.

Cyclic voltammetry was used to investigate the catalyst and its AOR activity (Fig. 4). The $Ni(OH)_2$ reference exhibits two redox peaks. The anodic peak is the overlapping $Ni^{2+}/Ni^{3+}$ oxidation peak and the OER activity, with an onset potential of 1.39 V *vs.* RHE. The reduction peak originates from the reduction of both γ-NiOOH to α-$Ni(OH)_2$ and β-NiOOH to β-$Ni(OH)_2$, with the γ-NiOOH reduction occurring at a more positive potential.[31] In general, γ-NiOOH is associated with higher attainable $Ni^{3+}$ to $Ni^{4+}$ valences, which are charge compensated by the anion and water incorporation in the layered structure. The incorporation of Cu results in a limited change in onset potential of the oxidation peak, but the current density is significantly reduced. Also in the Tafel plots in Fig. 5, it can be observed that the $NiCu_{0.2}$ has lower OER activity at the same applied potential. This lower OER activity is beneficial for suppressing the competing OER and can therefore increase the AOR FE. The cathodic peak shape is different from that of pure $Ni(OH)_2$, which seems to be related to more γ-$NiCu_{0.2}OOH$ reduction at a more positive reduction potential, compared to less β-$NiCu_{0.2}OOH$ reduction. This

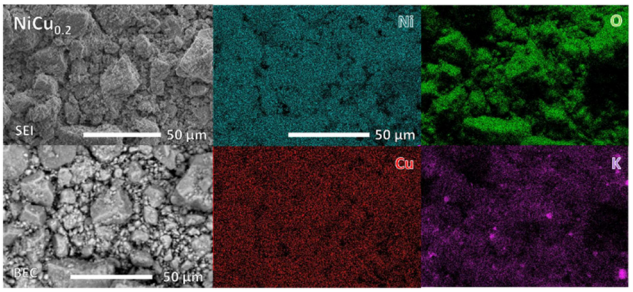


**Fig. 3** SEM and EDS images of $NiCu_{0.2}$ with separate images, indicating the presence of Ni, Cu, O and K. The inhomogeneous distribution of K correlates with sulphur and originates from the separated $K_2SO_4$ salt from the precipitation synthesis method. Both secondary electron imaging (SEI) and backscatter electron imaging (BEC) modes of SEM are applied to show topography and composition, respectively.

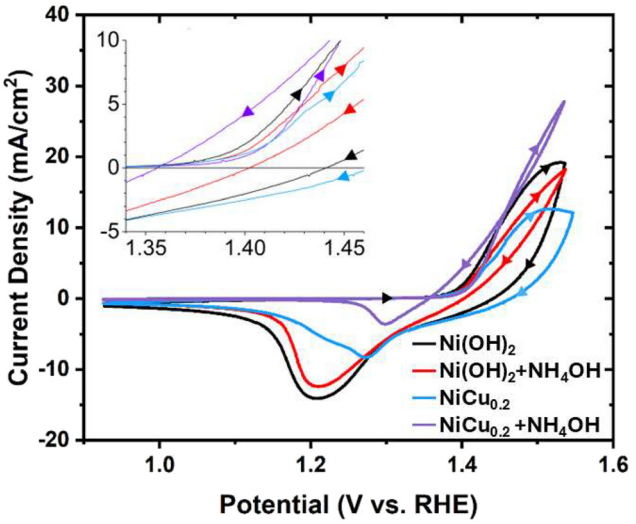


**Fig. 4** Cyclic voltammetry of $Ni(OH)_2$ and $NiCu_{0.2}$ in 1 M KOH with and without 50 mM $NH_4OH$. A scan rate of 1 mV $s^{-1}$ was used. The current densities refer to the geometric surface area.

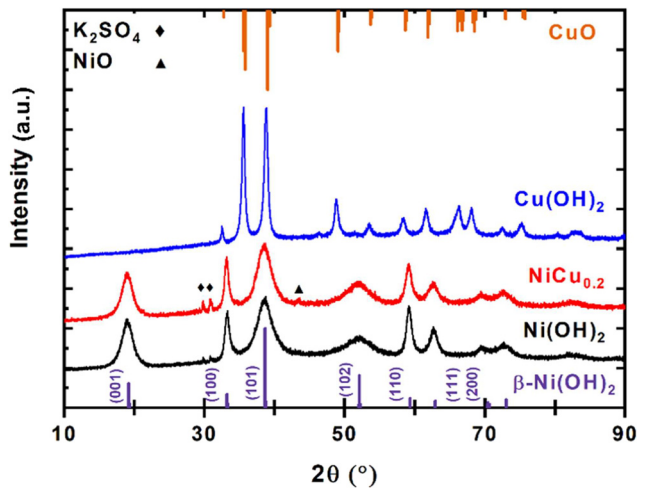


**Fig. 2** XRD pattern of $NiCu_{0.2}(OH)_2$ in comparison with those of β-$Ni(OH)_2$ and $Cu(OH)_2$ recorded through the same synthesis method. At the bottom, a β-$Ni(OH)_2$ (COD 1011134) reference pattern, and at the top, a CuO (COD 1011148) reference pattern, are shown. The $NiCu_{0.2}(OH)_2$ pattern closely resembles that of β-$Ni(OH)_2$.

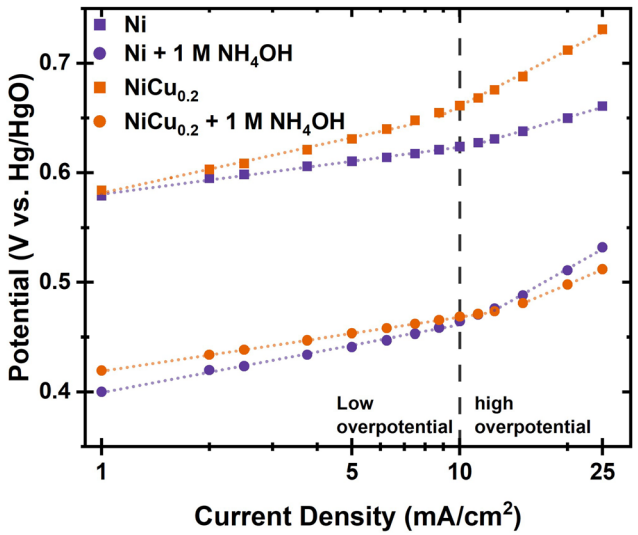


**Fig. 5** The Tafel plot of $Ni(OH)_2$ and $NiCu_{0.2}$ for the OER and the AOR in 1 M KOH with and without 1 M dissolved $NH_3$ based on a stepwise increase of current density to reduce error caused by gas bubble formation. The dashed line illustrates the divide between the low and high overpotential ranges.

suggests that significant phase conversion to γ-$NiCu_{0.2}OOH$ occurs during oxidation.

The addition of ammonia to the electrolyte resulted in a 10 mV reduction of onset potential for oxidation with β-$Ni(OH)_2$. However, the overall peak current density decreased, suggesting that $Ni(OH)_2$ has a limited AOR activity. The smaller reduction peak implies that AOR occurs, as less current is available for NiOOH formation. In contrast to $Ni(OH)_2$, $NiCu_{0.2}$ has an increased oxidation current density with a significant peak shape change in the presence of ammonia. Initially, the cathodic scan has a similar current density to the anodic scan, before surpassing it as it drops to zero at 1.35 V *vs.* RHE. This enhanced activity originates from the AOR on the oxyhydroxide formed during oxidation, and continues with an indirect AOR below the onset potential of the anodic scan, reforming oxyhydroxide back to hydroxide (eqn (5)). The smaller $NiCu_{0.02}OOH$ reduction peak with the presence of ammonia confirms this mechanism. These results indicate that the AOR is limited by the formation of NiOOH from $Ni(OH)_2$. The onset potential of the AOR is therefore equal to the potential of NiOOH formation.[20] The higher AOR activity will then be an intrinsic property of $NiCu_{0.2}$, which can be related to Cu with its valence limited to 2+, affecting the $Ni^{2+}:Ni^{3+}:Ni^{4+}$ ratio and the formation of $NiCu_{0.2}(OH)_2$ and β- and γ-$NiCu_{0.2}OOH$ or a mixed 'interstratified' phase.[20,24,32–36] The remaining cathodic peak is also at the more positive potential side, associated rather with γ-$NiCu_{0.2}OOH$ reduction to α-$NiCu_{0.2}(OH)_2$ than with β-$NiCu_{0.2}OOH$. This may indicate that especially the β-$NiCu_{0.2}OOH$ is active in the (indirect) AOR as the β-phase is apparently already reduced following eqn (5) before the cathodic sweep reaches its reduction potential in the absence of $NH_3$. Elucidation of the reaction mechanism is challenging and may require *in operando* XRD and EXAFS characterisation methods during the AOR to provide insight into the phase behaviour and state of Ni and Cu,[18] while *in operando* near ambient pressure XPS could potentially be used to observe relevant N species.[37]

Tafel plots were measured to further investigate the difference in the reaction kinetics between $Ni(OH)_2$ and $NiCu_{0.2}$. They were measured with an initial anodic current to convert all hydroxide material to oxyhydroxide, because NiOOH is the AOR active material. In the Tafel plot, a low and high overpotential range is observed (Fig. 5). At low current densities, the Tafel slopes are 43 and 72 mV $dec^{-1}$ for $Ni(OH)_2$ and $NiCu_{0.2}$, respectively. The difference is more significant in the high overpotential range, with 96 and 169 mV $dec^{-1}$, respectively. These higher Tafel slopes indicate a lower OER activity for $NiCu_{0.2}$, which should limit OER activity during ammonia oxidation, increasing the FE.

The addition of ammonia results in significant changes in both the Tafel slope and potential. At 10 mA $cm^{-2}$, we found a reduction of potential from 0.624 to 0.465 V and from 0.662 to 0.469 V *vs.* Hg/HgO for $Ni(OH)_2$ and $NiCu_{0.2}$, respectively. For $Ni(OH)_2$, this coincides with a Tafel slope increase to 62 mV $dec^{-1}$. In the high overpotential range, the Tafel slope changes to 186 mV $dec^{-1}$. The significant increase in slopes indicates sluggish AOR activity with intermediate coverage limiting the OER. In comparison, the Tafel slopes of $NiCu_{0.2}$ reduce to 49 and 140 mV $dec^{-1}$ for the low and high current density ranges, respectively. This explains the higher AOR activity measured with cyclic voltammetry. With this reduction in the Tafel slope, it can be expected that at high current densities, $NiCu_{0.2}$ will be able to maintain high AOR selectivity. This is a result of OER activity being limited by the higher onset potential and Tafel slope. Therefore, we will focus on $NiCu_{0.2}$ to evaluate the effect of experimental conditions and cell layout on the ammonia oxidation.

## Electrolyte and pH dependence of the ammonia oxidation reaction

High AOR activity has been exhibited by $NiCu_{0.2}$. Nonetheless, the supporting electrolyte and ammonia concentration can significantly influence the AOR selectivity and FE. Therefore, understanding the effect of electrolyte is crucial to achieve high FE and selectivity under industrial relevant conditions. The influence of the electrolyte was investigated in a single compartment cell (Fig. 1a) to establish the impact of the electrolyte composition and undivided cell. Each experiment started with achieving a stable potential without the presence of ammonia to form the active NiOOH material, before initiating the experiment with the addition of dissolved ammonia. This method removes apparent FE losses that are solely related to $Ni(OH)_2$ oxidation to NiOOH, representing a continuous industrial ammonia electrooxidation process. The nitrite and nitrate production was monitored while the latter concentration was negligible and is therefore omitted for clarity, unless relevant for discussion.

The application of 1 M $NH_4OH$ as the electrolyte resulted in a FE of 34% for the conversion of ammonia to nitrite in the initial 4 hours, with consistent nitrite formation (Fig. 6). However, after 22 hours, the nitrite concentration decreased. This agrees with our earlier statement regarding unobstructed access to the counter electrode resulting in reduction of nitrite, achieving an equilibrium concentration. In comparison, concentrated ammonia (28 wt%, 14.5 M) reduced the nitrite formation rate and a FE of 10% for the initial 4 hours was determined. After 22 hours, only a slight increase in nitrite concentration was observed, implying that the additional ammonia does not promote the reaction. Furthermore, a pH effect was observed. Medvedev *et al.* reported that $Ni(OH)_2$ switches to producing nitrate below pH 12.[38] This is near the pH of the electrolyte with values of 11.6 and 12.2 for 1 M and 14.5 M $NH_4OH$, respectively. The pH is further lowered with conversion of the basic ammonia to strong nitrous and nitric acids. This is confirmed by an increase in nitrate concentration to 0.16 and 0.29 mM after 22 hours for 1 M and 14.5 M ammonia, respectively.

The results indicate that the addition of an alkaline supporting electrolyte, KOH, is required to stabilize the pH. The addition of 1 M KOH to the 14.5 M $NH_4OH$ electrolyte resulted in no notable difference within the initial 4 hours. Despite this, after 22 hours, a higher nitrite concentration was established. In comparison, 1 M KOH and 1 M $NH_4OH$ combined had a significantly higher initial production rate, without noticeable end concentration difference. The initial rate would mainly depend on the direct catalytic effect, suggesting that ammonia or reaction intermediates block active sites with 14.5 M $NH_4OH$ limiting the rate. The addition of 1 M KOH to 1 M $NH_4OH$ promoted the AOR, suggesting that the higher pH is not detrimental to the AOR, rather an optimal ammonia concentration between 1 and 14.5 M exists. The similar higher end concentration originates from the $OH^-$ ion conductivity, reducing the transport number of nitrite and the correlated nitrite mobility and its (detrimental, nitrite loss making) reduction at the counter electrode. The KOH concentration was further increased to 6 M KOH with 1 M $NH_4OH$ to investigate if this can enhance nitrite production. However, the nitrite formation rate decreased, likely due to the reduced $NH_3$ solubility and increased vapor pressure with higher KOH concentration.[39] As a result, less $NH_3$ is available for oxidation within the electrolyte. The production rate was still linear for 4 hours, confirming that the FE loss does not originate from $NH_3$ loss over time. Therefore, we chose to continue with 1 M KOH and 1 M $NH_4OH$ for the following experiments, as it should result in the highest FE and stability (Fig. 7).

### Cation membrane integration for the increased yield and product separation

1 M KOH limits the experimental runtime due to the change in pH. Therefore, the experiment was repeated with 6 M KOH to determine if prolonged conversion could be achievable. Furthermore, the cell was reduced from 125 to 50 mL for each compartment to improve the performance. This reduction decreased the electrode gap, measuring time and ammonia vapour losses. The vapour loss was further reduced by limiting air contact through further sealing. The experiments were terminated when the initial OER potential, established before ammonia addition, was reached. This resulted in an insignificant ammonia concentration remaining, while preventing electrode damage from the reduced pH.

An H-cell divided by a Nafion 117 CEM wass chosen as the setup for preventing reduction of nitrite and nitrate at the counter electrode, as this has very limited nitrite and nitrate

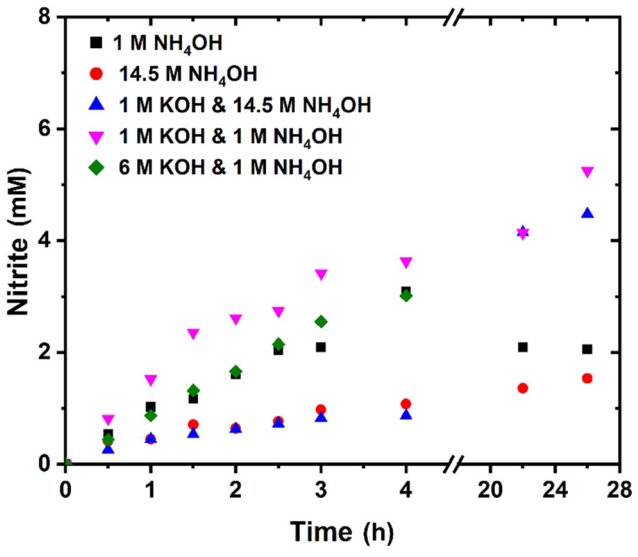


Fig. 6 Bulk electrochemical oxidation of ammonia under various conditions at 5 mA $cm^{-2}$ with $NiCu_{0.2}$ as the catalyst. Only the nitrite concentration is shown as the nitrate concentration was negligible unless otherwise mentioned.

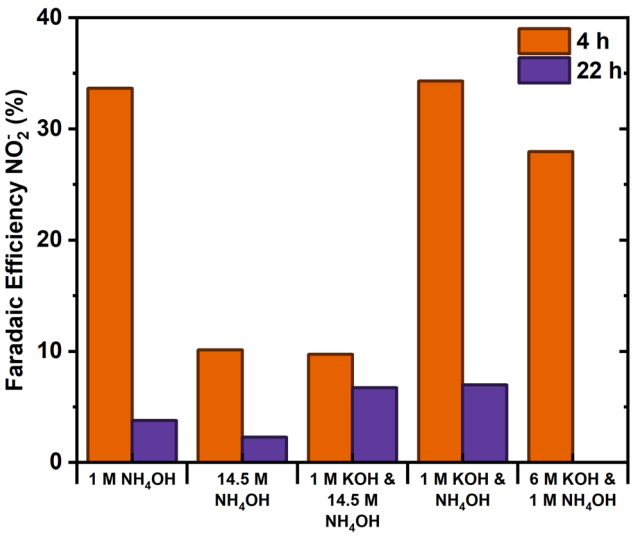


Fig. 7 Summary of the faradaic efficiency towards nitrite for the initial 4 hours and the total 22 hours of the abovementioned experiment within a single compartment cell with $NiCu_{0.2}$ at 5 mA $cm^{-2}$.

anion transport and high cation transport. In this case, the $K^+$ transport is dominant as it has a high concentration at 1 M KOH and protons are essentially absent. Ammonia was added to both sides of the membrane to mitigate ammonia crossover. The initial results achieved with this setup in 1 M KOH with 1 M $NH_3$ electrolyte at 10 mA $cm^{-2}$ were promising with a constant production of nitrite for 70 hours (Fig. 8a). This is a significantly longer runtime with constant production, resulting in a yield of 150 mM nitrite, demonstrating the detrimental effect of product reduction at the cathode in the absence of the membrane. After these initial 70 hours, the nitrate concentration increased exponentially due to the depletion of $OH^-$ and reduction of the pH to below 9. This coincided with an increase in potential due to the reduction of conductivity from the lower electrolyte concentration (Fig. 8b). The change in the pH and depletion of $OH^-$ is expected under alkaline conditions, because the CEM transfers $K^+$ through the membrane, while simultaneously $OH^-$ is consumed within the anolyte. $NH_4^+$ could also be transported as a cation; however, at the applied pH, its presence is suppressed in favour of neutral dissolved $NH_3$. The pH dependence of nitrite oxidation to nitrate was confirmed by performing an experiment in 1 M KOH with 1 M $KNO_2$ (Fig. S4). Only 33 mM nitrate was formed after 6 hours. When the measured oxidation potential had significantly increased, indicating the lowering of pH, almost complete conversion to nitrate was obtained. Therefore, maintaining a stable alkaline pH is crucial to achieve high nitrite selectivity.

The initial results with 6 M KOH in the electrolyte were obtained with a total operation time of 76 hours with minimal nitrate formation (Fig. 9). A lower FE of 52% at 2.5 mA $cm^{-2}$ towards nitrite was obtained, in comparison with 97% for the previous measurement with 1 M KOH at 10 mA $cm^{-2}$. The limited activity in 6 M KOH could originate from the limited formation rate of $NiCu_{0.2}OOH$ due to the lower potential at the applied current density. The reaction was initiated with a potential of 0.33 V *vs.* Hg/HgO. This is just above the $NiCu_{0.2}(OH)_2/NiCu_{0.2}OOH$ equilibrium potential for $NiCu_{0.2}(OH)_2$ at a low state of charge, indicating that a $NiCu_{0.2}OOH$ surface could be formed.[27,40,41] Also when comparing the experiment with a pure $Ni(OH)_2$ electrode (Fig. S5), the-Cu doped sample directly shows a higher potential but rather a lower rate as the AOR seems to be potential dependent. In combination with the CV scans in Fig. 4, we conclude that the current and resulting potential are high at the onset of AOR activity, while the increased AOR activity requires higher potentials. In addition, Fig. 5 shows the potential at the same low current density of the $NiCu_{0.2}$ sample to be higher than that for pure Ni, which would bring it closer to that for the OER. Thus, increasing the current density and the correlated potential should increase the $NiCu_{0.2}OOH$ formation rate and the subsequent AOR to nitrite, and move into a current and potential territory where the $NiCu_{0.2}$ in the presence of ammonia requires a lower potential for the same current. Therefore, to promote the AOR, the current density was increased to 25 mA $cm^{-2}$ (Fig. 10) and 1 M KOH was compared with 6 M KOH again. The 1 M KOH electrolyte had a limited runtime of 14 hours with a higher potential in comparison with 6 M KOH (Fig. 10b). Furthermore, the potential with 6 M KOH electrolyte was significantly lower than expected based on the pH difference (Fig. 10c). This is expected to originate from the AOR and will result in improved energy efficiency. In the initial 8 hours, the nitrite FE was 87% for 1 M KOH, slightly higher compared to 82% for 6 M KOH. However, the difference in FE is less significant than the potential reduction. The addition of ammonia resulted in a potential drop of 0.20 V with 1 M KOH, compared to 0.24 V with 6 M KOH. This effect was further demonstrated by the cell potential. The addition of ammonia reduced the potential to 2.67 V from 2.76 V with 1 M KOH, whereas a 12% reduction from 2.24 V to 2.08 V was

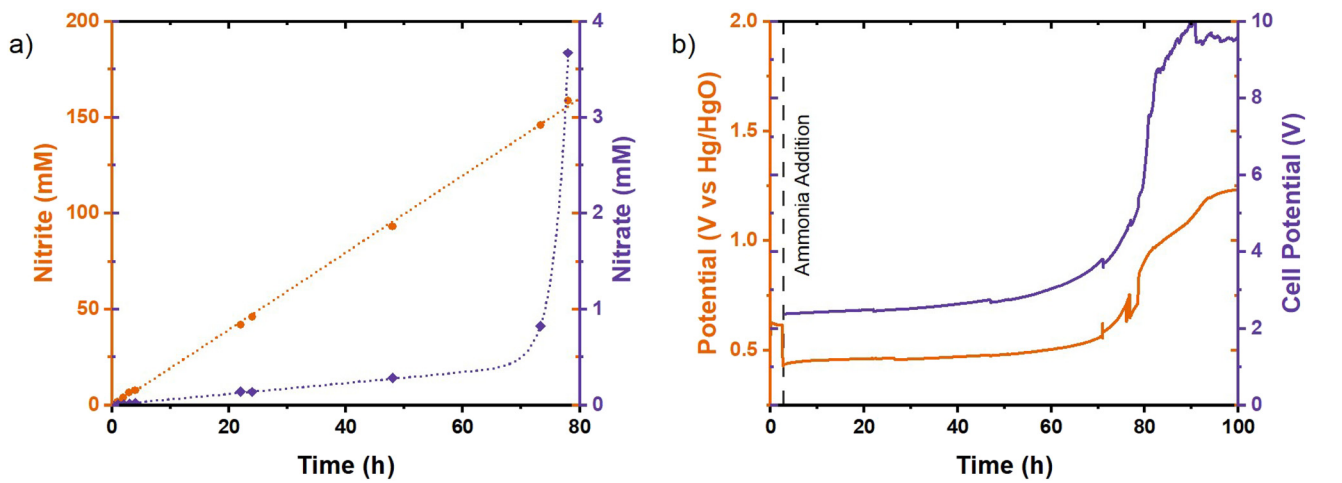


**Fig. 8** Chronopotentiometry of the $NiCu_{0.2}$ electrode performing the AOR in 1 M $NH_3$ in 1 M KOH at 10 mA $cm^{-2}$ in a glass H-cell divided by a Nafion 117 cation exchange membrane. (a) Concentration of products during chronopotentiometry and (b) the measured potentials. The left graph stops at 80 hours, as the results of the last 20 hours were not representative.

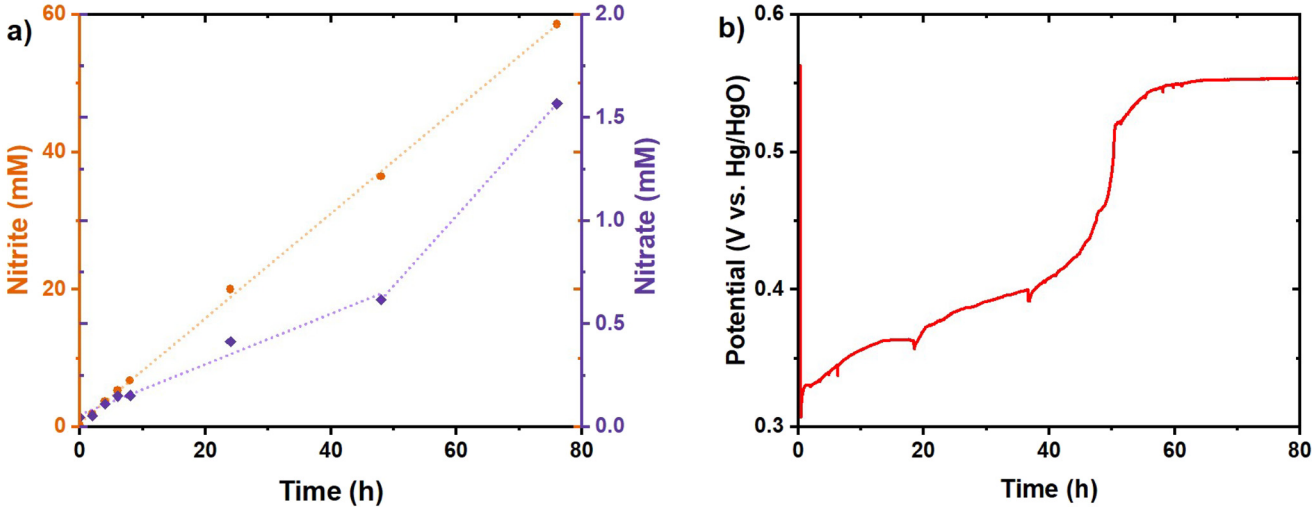


**Fig. 9** Chronopotentiometry of $NiCu_{0.2}$ in 6 M KOH with 1 M $NH_3$ at 2.5 mA $cm^{-2}$. (a) Measured nitrite and nitrate concentrations with the dashed lines showing linear trends. (b) The measured potential during the chronopotentiometry.

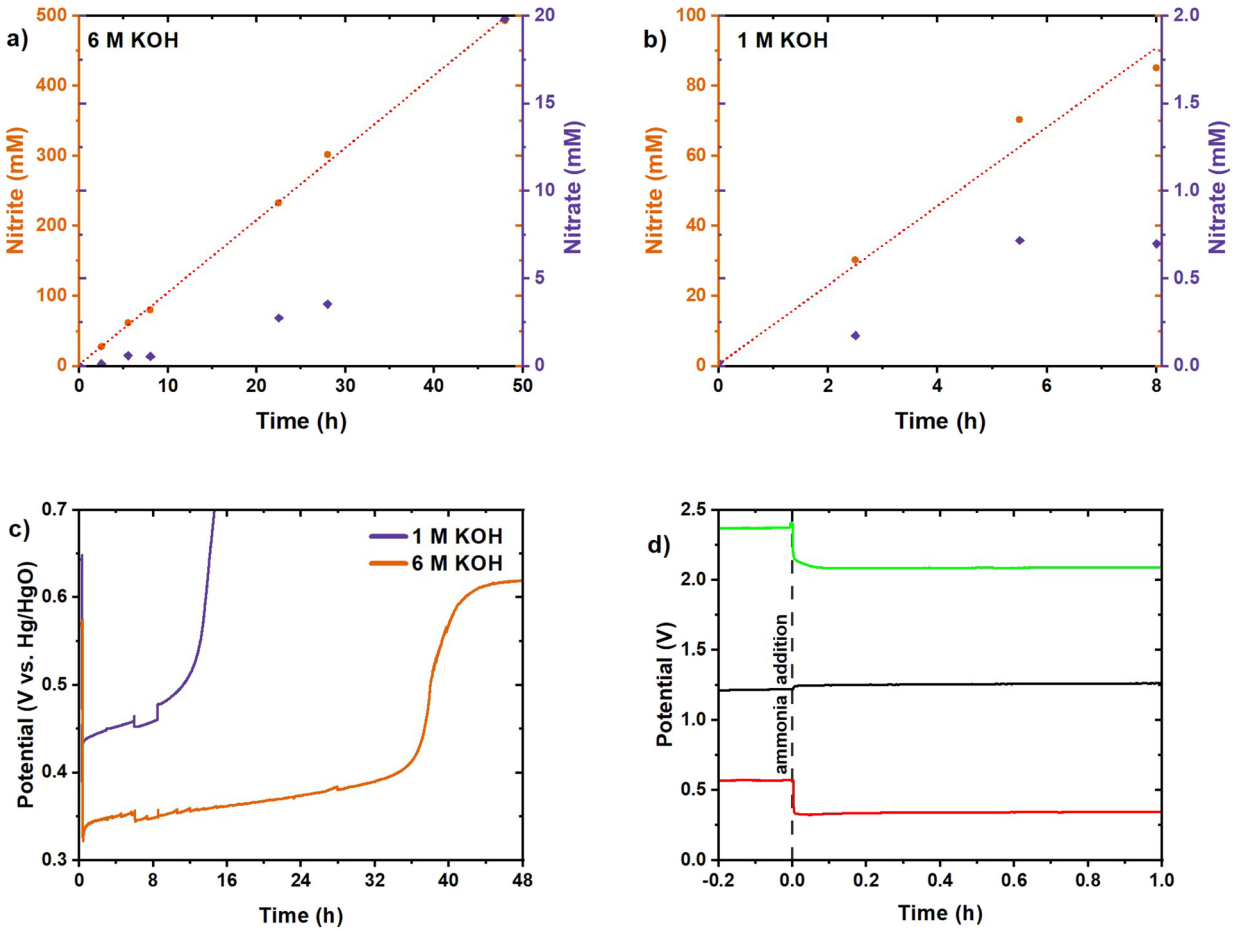


**Fig. 10** Product concentration for chronopotentiometry with $NiCu_{0.2}$ at 25 mA $cm^{-2}$ in the cation membrane-divided cell: (a) 1 M KOH with 1 M $NH_3$ and (b) 6 M KOH with 1 M $NH_3$. (c) Potential measured during the chronopotentiometry. (d) Absolute potentials measured during the chronopotentiometric measurement for the first hour in 6 M KOH with 1 M $NH_3$. Ammonia addition is illustrated with a dashed line. The working electrode (red) and counter electrode (black) were measured against their own reference electrode. The cell potential is marked in green.

recorded with 6 M KOH. These potentials are higher than the theoretical potential due to activation overpotentials, and the electrode gap and its resulting significant internal resistance. Furthermore, the prolonged stable activity with 6 M KOH resulted in 49% conversion after 48 hours with 78 and 4% FE towards nitrite and nitrate, respectively. These promising results suggested a further increase of the current density as that could result in even higher FE as we approach an industrially relevant current density.

To further prove the feasibility of industrial electrochemical ammonia oxidation, the current density was increased to 400 mA $cm^{-2}$. Within less than 3.5 hours, 769 mM of ammonia was converted to nitrite and nitrate (Fig. 11a). The initial OER potential of 0.80 V *vs.* Hg/HgO reduced to an AOR potential of 0.60 V *vs.* Hg/HgO upon ammonia addition (Fig. 11c). The limited potential decrease of 20 mV from the counter electrode suggests a minimal poisoning effect on hydrogen evolution. A total cell potential of 2.0 V was calculated, ignoring internal resistances. The theoretical equilibrium cell potential should be 1.3 V, the difference between eqn (6) and (8), as (2) only occurs when NiOOH is present. A significant difference originates from the non-optimised counter electrode and the high overpotential. Further cell optimisation outside this study is required to actually reach reduced potentials closer to the equilibrium potential. At the higher applied current density and potential, a nitrite FE of 91% and a total FE of 95% were achieved (Fig. 11b). Meanwhile, the potential exceeded the onset potential of the OER but did not result in significant OER activity. Ammonia and AOR intermediates limit $O_2$ formation while enhancing nitrite formation. This occurs either by occupying actives sides with intermediates and ammonia or by reacting with the OER intermediates.[42] The OER requires the formation of NiOOH, which is rapidly consumed through an indirect AOR when locally present. This agrees with the lower AOR Tafel slope of $NiCu_{0.2}$, indicating higher activity for the AOR than the OER.

## Comparison with previous results

As stated in the Introduction section, a comparison with the literature for AOR catalysts is presented in Table S1. The AOR towards nitrite and nitrate is reported mostly for Cu and Ni or Co based catalysts, while noble metal-based catalysts mostly yield $N_2$. The yields of nitrate and nitrite show a maximum FE of above 86% for the applied current density of 2 mA $cm^{-2}$. The maximum current density applied of ~100 mA $cm^{-2}$ yields about 5% FE conversion to nitrite. The presently observed 400 mA $cm^{-2}$ and FE of 96% therefore advance the AOR significantly towards industrially relevant values.

Direct comparison is difficult because the Ni–Cu based materials are reported to be inhomogeneous mixtures of Ni $(OH)_2$ and $Cu(OH)_2$, or Cu–Ni metal alloys. The latter will have an oxidised (oxy-)hydroxide surface since the potentials applied are well above their oxidation potentials. Also, note that their AOR potentials are above the OER/ORR *vs.* RHE (eqn (7)), and therefore more positive than the equilibrium potentials of eqn (1)–(3), excluding spontaneous fuel cell operation. The published onset potential changes in a representative example by Xu *et al.* are small in comparison with *in situ*-grown inhomogeneously mixed $Ni(OH)_2$- and $Cu(OH)_2$-based nanowires with and without ammonia.[24] This is also the case for the $Ni(OH)_2$ and $NiCu_{0.2}$ reported here as the oxyhydroxide formation determines the onset potential. In addition, the Tafel slopes with 55 mM $NH_4^+$ concentration are similar to those observed with 1 M $NH_3$. However, in ref. 24, the current density saturated above a concentration of 150 mM, which means lower currents in the Tafel experiment at higher concentrations. The reported oxidation product at their attainable 9 mA $cm^{-2}$ after 24 h is about 19% FE nitrate, while now with the homogeneously prepared $NiCu_{0.2}$, we report below constant current densities up to 400 mA $cm^{-2}$ and high FE conversion to nitrite. Also, pure $Ni(OH)_2$ is reported in membrane-separated cells to reach promising AOR activities up to ~30 mA $cm^{-2}$ with 0.2 M $NH_4OH$, but with still significant $N_2$ production (20–90% FE) next to nitrite and nitrate yields that

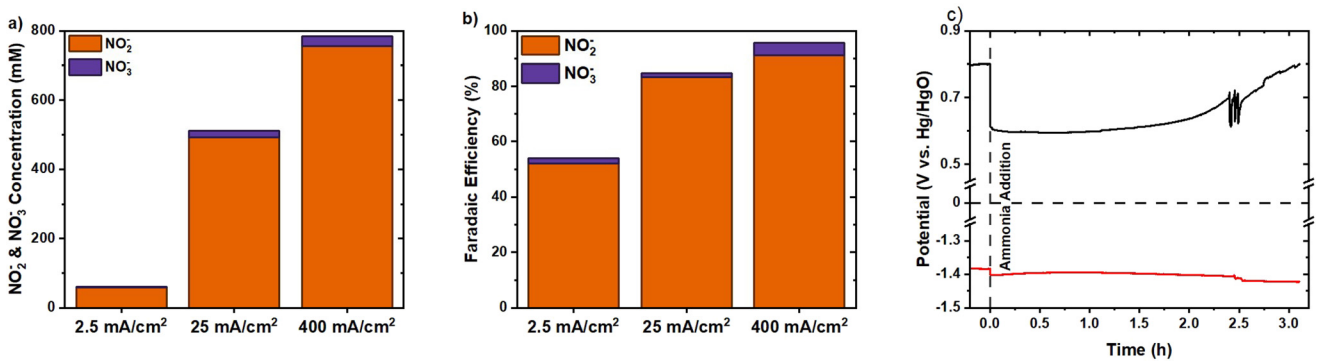


**Fig. 11** AOR in a cation membrane-divided cell. (a) Nitrite and nitrate concentrations for the chronopotentiometric measurement with $NiCu_{0.2}$, at the end measured in 6 M KOH with 1 M $NH_3$ at various current densities. (b) Summary of the faradaic efficiency achieved for the chronopotentiometric methods with increasing current density. (c) Measured potential at a current density of 400 mA $cm^{-2}$ for the working electrode (black) and the counter electrode (red) against their own reference electrode in their compartment.

depend on the pH. The OER will make up the missing current amounts at the applied potentials.

### Electrode stability

Long-term stability of the electrode material is fundamental to ensure cost-effective industrial application. The XRD pattern of the used electrode is comparable to that of the original powder, with the β-$Ni(OH)_2$ phase as the main contributor (Fig. 12). Additional peaks correspond to the nickel foam, graphitic carbon, $KOH{\cdot}2H_2O$ and $KHCO_3$. Furthermore, no separated copper oxide or peak shift was detected, indicating a limited change within the crystalline material.

Potential corrosion structural changes and the change in composition were determined using SEM and EDS. The used electrode (Fig. 13) displayed macroscale cracking in comparison with the unused electrode (Fig. S1). However, the Ni current collector remains largely covered, with limited loss of $NiCu_{0.2}$ particles. The BED modus confirms the equivalent size and distribution of the $NiCu_{0.2}$ material in the pristine and used electrodes. Additional particles were identified as $KOH{\cdot}2H_2O$ and $KHCO_3$ salts in accordance with XRD. EDS analysis reported a composition of $NiCu_{0.04}$ for the electrode produced initially with $NiCu_{0.2}$ particles. Therefore, under the alkaline oxidative conditions from the experiments, a significant amount of Cu dissolved. Nonetheless, the remaining Cu concentration suggests resistance to further corrosion. Such Cu dissolution and corrosion could result in copper complexes that are relatively stable, as indicated in eqn (9)–(11).[43,44]

$$Cu^{2+} + 2OH^- \rightleftarrows CuO_{(s)} + H_2O \quad (9)$$

$$3Cu^{2+} + 4OH^- \rightleftarrows Cu_3(OH)_4^{2+} \quad (10)$$

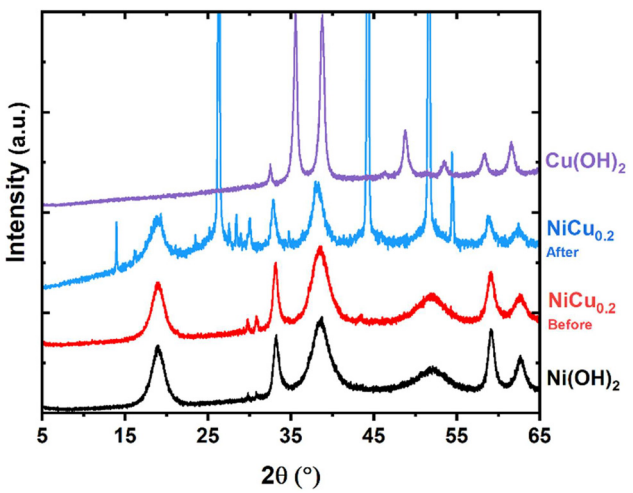


**Fig. 12** XRD pattern of $NiCu_{0.2}$ used for the experiment with 6 M KOH and 1 M $NH_3$ at 400 mA $cm^{-2}$ for close to 3.5 hours. $Ni(OH)_2$ and $Cu(OH)_2$ powders were added as references for related peaks. The four biggest sharp peaks originate from graphitic carbon and nickel present in the electrode. $NiCu_{0.2}$ powder was added for comparison of the phase and potential peak changes.

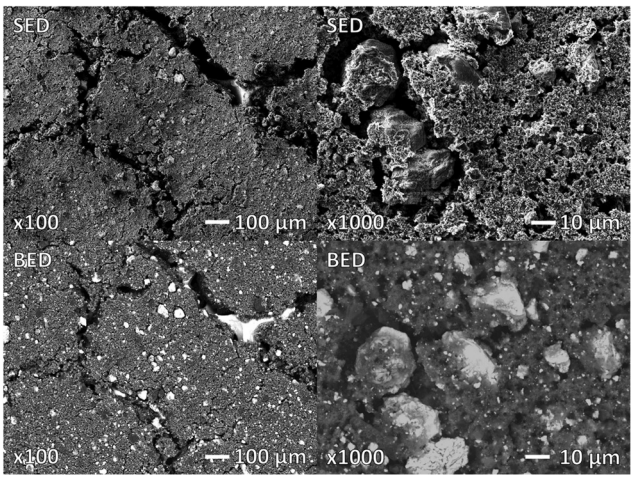


**Fig. 13** SEM after the application of 400 mA $cm^{-2}$ during experiments in Fig. 11. This shows the limited effect of the experiments on the $NiCu_{0.2}$ containing electrode in comparison with Fig. S1. Both secondary electron detector (SED) and backscatter electron detector (BED) modes of SEM are applied to show topography and composition, respectively.

$$Cu^{2+} + 2NH_3 + 2OH^- \rightleftarrows Cu(NH_3)_2(OH)_2 \quad (11)$$

In a forthcoming publication, we will report on this $NiCu_{0.04}$ stable composition resulting after prolonged oxidation in 6 M KOH and compare it with DFT calculations, indicating its stability against dissolution as shown in eqn (9)–(11). However, here we note that even in the presence of ammonia and nitrite, $NiCu_{0.04}$ shows stable composition during prolonged experiments at industrial current densities.

### Dual product electrolyser

This study demonstrated that it is possible to achieve high FE within 1 M $NH_3$ with selective conversion of ammonia to $NO_2^-$. This significant reduction in potential in comparison with the OER presents a possible method for reducing the potential of an electrolyser, while making a value-added product, rather than the oxygen waste product. However, this requires ammonia in the catholyte, which makes product purification more complex. The setup can be further optimized by balancing the $K^+$ transport through the CEM by flowing the catholyte into the anolyte (Fig. 14). The nitrite could further be used as a fertilizer, while the $H_2$ could be used for energy storage or reinvested in the production of the consumed $NH_3$.

Overall, this system could be interesting for small scale synthetic fertilizer production, especially if local electricity is produced in excess due to intermittence. The end product could be either $KNO_2$ or $NH_4NO_2$, both of which are of value for contributing to the NPKS (nitrogen, phosphor, potassium, and sulphur) ratio of synthetic fertilizers. With KOH balanced within the system, the only input is ammonia, water, and KOH to compensate for product removal. The electrolyte could even be used directly if the pH is balanced through the addition of phosphoric acid and sulfuric acid. The addition of these acids would contribute to the NPKS ratio of the fertilizer. Farmers

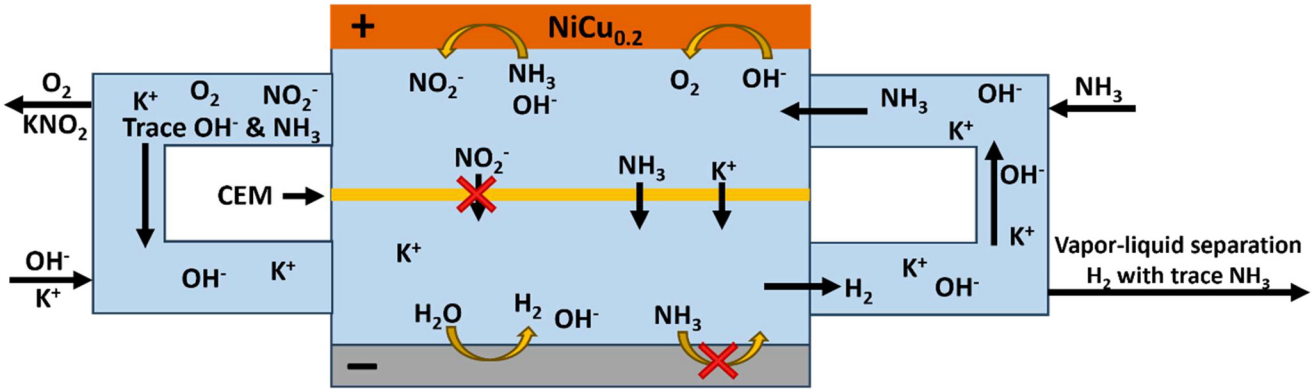


**Fig. 14** Schematic diagram of an AOR flow cell with a central liquid flow, resulting in cycling of $K^+$ through the membrane. At the bottom negative electrode, water reduction takes place, producing $H_2$ and $OH^-$. Charge compensating $K^+$ is transported through the CEM rather than protons under alkaline conditions. At the positive electrode, $NH_3$ oxidation to $NO_2^-$ occurs using $OH^-$ (and trace water oxidation to $O_2$). The KOH and $NH_3$ input flow channels provide feeds to enable the overall reaction $KOH + H_2O + NH_3 \rightarrow KNO_2 + 3H_2$, as well as the (undesirable) OER. Ammonium could be transported back into the bottom cell, if the pH permits its presence (*e.g.*, at the outlet for $KNO_2$ where $OH^-$ becomes depleted).

would then be able to produce their own specific ratio with limited transport costs and shorter supply chains. Furthermore, this would limit the storage and transport of ammonium nitrate, which is a potentially hazardous substance.

## Conclusions

$Ni_{0.8}Cu_{0.2}(OH)_2$ has been investigated as a potential catalyst for ammonia oxidation to nitrite at industrially relevant current densities and concentrations. The Cu was homogeneously incorporated within the β-$Ni(OH)_2$ phase to enhance the catalytic properties of $Ni(OH)_2$. The prepared $Ni_{0.8}Cu_{0.2}$ has lower Tafel slopes of 49 and 140 mV $dec^{-1}$ at lower and higher current densities, respectively, compared to 62 and 186 mV $dec^{-1}$ for the undoped $Ni(OH)_2$. In an undivided cell, the nitrite and nitrate yields are limited by the re-reduction of these products on the cathode. Furthermore, pH stabilisation with a supporting alkaline electrolyte is required to prevent pH reduction, which would also enable nitrite to nitrate oxidation.

In comparison, a Nafion® 117 cation exchange membrane divided cell under alkaline conditions results in consistent nitrite formation. This is only limited by ammonia depletion and the reduction of the pH to below 12. With this setup, the ammonia oxidation performance of $NiCu_{0.2}$ significantly improved with respect to the yield and current densities. A faradaic efficiency towards nitrite of 67% at 2.5 mA $cm^{-2}$ was achieved with 1 M ammonia in 6 M KOH. Furthermore, increasing the current density to 400 mA $cm^{-2}$ improved the total faradaic efficiency to 96% with 95% $NO_2^-$ : $NO_3^-$ selectivity. This was achieved with 77% conversion in less than 3.5 hours. It was observed that the original $Ni_{0.83}Cu_{0.17}$ content was reduced in Cu content to $Ni_{0.96}Cu_{0.04}$ by the continuous ammonia oxidation. However, this composition is expected to remain stable, as it has also been observed in long term operation. The setup could be further optimised for synthetic fertilizer production, enabling small-scale fertilizer manufacture. To conclude, we have successfully developed a copper-doped nickel hydroxide material that achieves promising results under industrial relevant current density and $NH_3$ concentration conditions. We suggest the application of a cation exchange membrane in future ammonia oxidation research to avoid skewing data towards $N_2$ formation.

## Author contributions

Conceptualization: FM and DvN. Data acquisition and curation: DvN and PJ. Writing – original draft: DvN, PJ, and FM. Review and editing: DvN, PJ, AU, and FM. Funding acquisition: FM.

## Conflicts of interest

There are no conflicts to declare.

## Data availability

Data for this article are available at https://data.4tu.nl/datasets/eeb4617c-4c92-45d1-a0ab-57e41fb8889b/1.

## Acknowledgements

This research was funded by the Nitrogen Activation and Ammonia Oxidation Project within the Electron to Chemical Bonds Consortium with project number P17-08, which is financed by The Netherlands Organization for Scientific Research (NWO) and affiliated industrial partners.

## References


1 *Fertilizer Industry Handbook 2022*, YARA, 2022.
2 J. Lim, C. A. Fernández, S. W. Lee and M. C. Hatzell, Ammonia and Nitric Acid Demands for Fertilizer Use in 2050, *ACS Energy Lett*, 2021, **6**, 3676–3685.
3 D. Chanda, R. Xing, T. Xu, Q. Liu, Y. Luo, S. Liu, R. A. Tufa, T. H. Dolla, T. Montini and X. Sun, Electrochemical nitrogen reduction: Recent progress and prospects, *Chem. Commun.*, 2021, **57**, 7335–7349.
4 Z. Huang, M. Rafiq, A. R. Woldu, Q.-X. Tong, D. Astruc and L. Hu, Recent progress in electrocatalytic nitrogen reduction to ammonia (NRR), *Coord. Chem. Rev.*, 2023, **478**, 214981.
5 X. Yang, S. Mukherjee, T. O'Carroll, Y. Hou, M. R. Singh, J. A. Gauthier and G. Wu, Achievements, challenges, and perspectives on nitrogen electrochemistry for carbon-neutral energy technologies, *Angew. Chem.*, 2023, **135**, e202215938.
6 P. Jungbacker, R. Kortlever and F. M. Mulder, Electrochemical nitrogen oxide formation from ammonia and dinitrogen, *Green Chem.*, 2026, **28**, 737–746, DOI: 10.1039/D5GC05480J.
7 K. H. R. Rouwenhorst, F. Jardali, A. Bogaerts and L. Lefferts, From the Birkeland–Eyde process towards energy-efficient plasma-based NOX synthesis: a techno-economic analysis, *Energy Environ. Sci.*, 2021, **14**, 2520–2534.
8 M. Thiemann, E. Scheibler and K. W. Wiegand, in *Ullmann's Encyclopedia of Industrial Chemistry*, John Wiley & Sons, Ltd, 2000.
9 W. Laue, M. Thiemann, E. Scheibler and K. W. Wiegand, in *Ullmann's Encyclopedia of Industrial Chemistry*, John Wiley & Sons, Ltd, 2000.
10 K.-W. Kim, Y.-J. Kim, I.-T. Kim, G.-I. Park and E.-H. Lee, Electrochemical conversion characteristics of ammonia to nitrogen, *Water Res.*, 2006, **40**, 1431–1441.
11 Y. Wang, Y. Yu, R. Jia, C. Zhang and B. Zhang, Electrochemical synthesis of nitric acid from air and ammonia through waste utilization, *Natl. Sci. Rev.*, 2019, **6**, 730–738.
12 J. Cui, J. Hou, H. Pan and P. Kang, Self-supporting CuM LDH (M = Ni, Fe, Co) carbon cloth electrodes for selective electrochemical ammonia oxidation to nitrogen, *J. Electroanal. Chem.*, 2023, **940**, 117502.
13 M.-H. Tsai, T.-C. Chen, Y. Juang, L.-C. Hua and C. Huang, High catalytic performance of CuCo/nickel foam electrode for ammonia electrooxidation, *Electrochem. Commun.*, 2020, **121**, 106875.
14 G. Zhang, J. Ruan and T. Du, Recent advances on photocatalytic and electrochemical oxidation for ammonia treatment from water/wastewater, *ACS ES&T Eng.*, 2021, **1**, 310–325.
15 G. Jeerh, M. Zhang and S. Tao, Recent progress in ammonia fuel cells and their potential applications, *J. Mater. Chem. A*, 2021, **9**, 727–752.
16 Z.-H. Lyu, J. Fu, T. Tang, J. Zhang and J.-S. Hu, Design of ammonia oxidation electrocatalysts for efficient direct ammonia fuel cells, *EnergyChem*, 2023, **5**, 100093.
17 P. Zou, S. Chen, R. Lan, J. Humphreys, G. Jeerh and S. Tao, Investigation of perovskite oxide $SrFe_{0.8}Cu_{0.1}Nb_{0.1}O_{3-\delta}$ as cathode for a room temperature direct ammonia fuel cell, *Int. J. Hydrogen Energy*, 2019, **44**, 26554–26564.
18 Y. Huan, Y. He, S. Liu, Q. Cheng, F. Zhou, J. Wang, M. Wang, C. Yan and T. Qian, Electrochemical ammonia oxidation reaction on nickel-based non-noble metal electrocatalysts: From mechanistic understanding to practical applications, *Adv. Energy Mater.*, 2025, **15**, e03815.
19 S. Cohen, S. Johnston, C. K. Nguyen, T. D. Nguyen, D. A. Hoogeveen, D. V. Zeil, S. Giddey, A. N. Simonov and D. R. MacFarlane, A $CoO_xHy$/β-NiOOH electrocatalyst for robust ammonia oxidation to nitrite and nitrate, *Green Chem.*, 2023, **25**, 7157–7165.
20 X. Jiang, D. Ying, X. Liu, M. Liu, S. Zhou, C. Guo, G. Zhao, Y. Wang and J. Jia, Identification of the role of Cu site in Ni-Cu hydroxide for robust and high selective electrochemical ammonia oxidation to nitrite, *Electrochim. Acta*, 2020, **345**, 136157.
21 S. Johnston, S. Cohen, C. K. Nguyen, K. N. Dinh, T. D. Nguyen, S. Giddey, C. Munnings, A. N. Simonov and D. R. MacFarlane, A survey of catalytic materials for ammonia electrooxidation to nitrite and nitrate, *ChemSusChem*, 2022, **15**, e202200614.
22 S. Johnston, L. Kemp, B. Turay, A. N. Simonov, B. H. R. Suryanto and D. R. MacFarlane, Copper-catalyzed electrosynthesis of nitrite and nitrate from ammonia: Tuning the selectivity via an interplay between homogeneous and heterogeneous catalysis, *ChemSusChem*, 2021, **14**, 4793–4801.
23 A. Kapałka, A. Cally, S. Neodo, C. Comninellis, M. Wächter and K. M. Udert, Electrochemical behavior of ammonia at $Ni/Ni(OH)_2$ electrode, *Electrochem. Commun.*, 2010, **12**, 18–21.
24 W. Xu, R. Lan, D. Du, J. Humphreys, M. Walker, Z. Wu, H. Wang and S. Tao, Directly growing hierarchical nickel-copper hydroxide nanowires on carbon fibre cloth for efficient electrooxidation of ammonia, *Appl. Catal., B*, 2017, **218**, 470–479.
25 F. Almomani and M. A. H. S. Saad, Electrochemical oxidation of ammonia ($NH_4$+/$NH_3$) ON synthesized nickel–cobalt oxide catalyst, *Int. J. Hydrogen Energy*, 2021, **46**, 4678–4690.
26 M. Zhu, Y. Yang, S. Xi, C. Diao, Z. Yu, W. S. V. Lee and J. Xue, Deciphering $NH_3$ adsorption kinetics in ternary Ni–Cu–Fe oxyhydroxide toward efficient ammonia oxidation reaction, *Small*, 2021, **17**, 2005616.
27 A. Iranzo and F. M. Mulder, Nickel-iron layered double hydroxides for an improved Ni/Fe hybrid battery-electrolyser, *Mater. Adv.*, 2021, **2**, 5076–5088.
28 P.-P. R. M. L. Harks, C. B. Robledo, C. George, C. Wang, T. van Dijk, L. Sturkenboom, E. D. W. Roesink and F. M. Mulder, Immersion precipitation route towards high


 

performance thick and flexible electrodes for Li-ion batteries, *J. Power Sources*, 2019, **441**, 227200.
29 P. Karanth, M. Weijers, P. Ombrini, D. Ripepi, F. Ooms and F. M. Mulder, A phase inversion strategy for low-tortuosity and ultrahigh-mass-loading nickel-rich layered oxide electrodes, *Cell Rep. Phys. Sci.*, 2024, **5**, 101972.
30 B. Izelaar, D. Ripepi, D. D. van Noordenne, P. Jungbacker, R. Kortlever and F. M. Mulder, Identification, quantification, and elimination of $NO_x$ and $NH_3$ impurities for aqueous and Li-mediated nitrogen reduction experiments, *ACS Energy Lett.*, 2023, **8**, 3614–3620.
31 N. I. Watson, M. Keegan, B. van den Bosch, N. Yan and G. Rothenberg, The influence of metal impurities on NiOOH electrocatalytic activity in the oxygen evolution reaction, *ChemElectroChem*, 2024, **11**, e202400223.
32 M. A. Ahsan, A. R. Puente Santiago, Y. Hong, N. Zhang, M. Cano, E. Rodriguez-Castellon, L. Echegoyen, S. T. Sreenivasan and J. C. Noveron, Tuning of trifunctional NiCu bimetallic nanoparticles confined in a porous carbon network with surface composition and local structural distortions for the electrocatalytic oxygen reduction, oxygen and hydrogen evolution reactions, *J. Am. Chem. Soc.*, 2020, **142**, 14688–14701.
33 W. Xu, D. Du, R. Lan, J. Humphreys, D. N. Miller, M. Walker, Z. Wu, J. T. S. Irvine and S. Tao, Electrodeposited NiCu bimetal on carbon paper as stable non-noble anode for efficient electrooxidation of ammonia, *Appl. Catal., B*, 2018, **237**, 1101–1109.
34 M.-H. Tsai, Y. Juang, C.-C. Hu, L.-C. Hua, B. K. Mahata and C. Huang, The direct electrocatalytic oxidation of ammonia by copper-deposited nickel foam catalysts, *Electrochim. Acta*, 2023, **446**, 142130.
35 M. Zhang, J. Zhang, G. Jeerh, P. Zou, B. Sun, M. Walker, K. Xie and S. Tao, A symmetric direct ammonia fuel cell using ternary NiCuFe alloy embedded in a carbon network as electrodes, *J. Mater. Chem. A*, 2022, **10**, 18701–18713.
36 E. Latvytė, X. Zhu, L. Wu, R. Lan, P. Vale and J. E. Graves, A low-temperature ammonia electrolyser for wastewater treatment and hydrogen production, *Int. J. Hydrogen Energy*, 2024, **52**, 265–282.
37 D. Ripepi, B. Izelaar, D. D. van Noordenne, P. Jungbacker, M. Kolen, P. Karanth, D. Cruz, P. Zeller, V. Pérez-Dieste, I. J. Villar-Garcia, W. A. Smith and F. M. Mulder, In situ study of hydrogen permeable electrodes for electrolytic ammonia synthesis using near ambient pressure XPS, *ACS Catal.*, 2022, **12**, 13781–13791.
38 J. J. Medvedev, Y. Tobolovskaya, X. V. Medvedeva, S. W. Tatarchuk, F. Li and A. Klinkova, Pathways of ammonia electrooxidation on nickel hydroxide anodes and an alternative route towards recycled fertilizers, *Green Chem.*, 2022, **24**, 1578–1589.
39 G. Cacciola, G. Restuccia and Y. Aristov, Vapor pressure of (potassium hydroxide + ammonia + water) solutions, *J. Chem. Eng. Data*, 1995, **40**, 267–270.
40 R. Barnard, C. F. Randell and F. L. Tye, Studies concerning charged nickel hydroxide electrodes I. Measurement of reversible potentials, *J. Appl. Electrochem.*, 1980, **10**, 109–125.
41 V. Srinivasan, J. W. Weidner and R. E. White, Mathematical models of the nickel hydroxide active material, *J. Solid State Electrochem.*, 2000, **4**, 367–382.
42 X. Xie, L. Du, L. Yan, S. Park, Y. Qiu, J. Sokolowski, W. Wang and Y. Shao, Oxygen evolution reaction in alkaline environment: Material challenges and solutions, *Adv. Funct. Mater.*, 2022, **32**, 2110036.
43 X. Wang, Q. Chen, H. Hu, Z. Yin and Z. Xiao, Solubility prediction of malachite in aqueous ammoniacal ammonium chloride solutions at 25 °C, *Hydrometallurgy*, 2009, **99**, 231–237.
44 I. Puigdomenech and C. Taxén, *Thermodynamic Data for Copper*, Svensk Kärnbränslehantering AB, 2000.